Supporting Information.

Solution Properties and Practical Limits of Concentrated Electrolytes for Nonaqueous Redox Flow Batteries.

Jingjing Zhang, [1,2] R. E. Corman [1,3] Jonathon K. Schuh, [1,3] Randy H. Ewoldt, [1,3] Ilya A. Shkrob, [1,2*] and Lu Zhang [1,2]

[1] *Joint Center for Energy Storage Research, Argonne National Laboratory, 9700 S. Cass Ave., Argonne, Illinois, 60439, USA*
[2] *Chemical Sciences and Engineering Division, Argonne National Laboratory, 9700 S. Cass Ave., Argonne, Illinois, 60439, USA*
[3] *Department of Mechanical Science and Engineering, University of Illinois at Urbana-Champaign, 405 N. Mathews Ave., Urbana, Illinois 61801, USA*

**** Corresponding author:*** Ilya A. Shkrob, e-mail shkrob@anl.gov, Tel. (630)2529516.

Abbreviations (except for chemical compounds, see Table S1 for the latter).

DOSY	diffusion ordered NMR spectroscopy
EPR	electron paramagnetic resonance
Lasso	least absolute shrinkage and selection operator
MMLR	multivariate multiple linear regression
NMR	nuclear magnetic resonance
NRFB	non-aqueous RFB
PGSE	pulsed-field gradient stimulated spin-echo NMR
QSPR	quantitative structure-property relationships
RFB	redox flow battery
ROM	(neutral) redox-active organic molecule
SOC	state of charge

Table S1. Abbreviations for Chemical Compounds.

BETI$^-$	$N(SO_2C_2F_5)_2^-$
BOB$^-$	*bis*(oxalato)borate
BzNSN	2,1,3-benzothiazole
BzNNN$^-$	benzotriazolide (mimic of $A^{-\bullet}$)
BzNCN$^-$	benzoimidazolide (mimic of $A^{-\bullet}$)
C	catholyte, 1-dimethoxyethoxy-2,5-di-*tert*-butyl-4-methoxy benzene
$C_n$mim$^+$	1-*n*-alkyl-3-methylalkylimidazolium
DCA$^-$	dicyanamide, $N(CN)_2$
DFOB$^-$	difluorooxalatoborate
FSI$^-$	$N(SO_2F)_2^-$
N_{abcd} $^+$	*a*,*b*,*c*,*d*-tetra(*n*-alkyl)ammonium
4MePyBu$^+$	4-methyl-1-*n*-butylpyridinium
$P_{1,4}$ $^+$	1-methyl-1-*n*-butylpyrrolidinium
MeImBz$^+$	1-benzyl-3-methylimidazolium
4[x]PyBz$^+$	4-[x]-1-benzylpyridinium
PyOc$^+$	*n*-octylpyridinium
S_{abc} $^+$	*a*,*b*,*c* -tri(*n*-alkyl)sulfonium
TDI $^-$	2-trifluoromethyl-4,5-dicyanoimidazolide
TFSI$^-$	$N(SO_2CF_3)_2^-$
THF	tetrahydrofuran

Scheme S1. Bond distances (*in green*, Å), bond angles (*in pink*, degree), and atomic Mulliken charges (*in red*) of 5-atom rings in the geometry optimized C_{2v} symmetrical $BzNSN^{-\bullet}$ anion and two closed shell mimics $BzNNN^-$ and $BzNCN^-$ in Scheme 2 according to our gas phase density functional calculations (B3LYP/6-31+G(d,p)). Shown below are the structural models for these three anions.

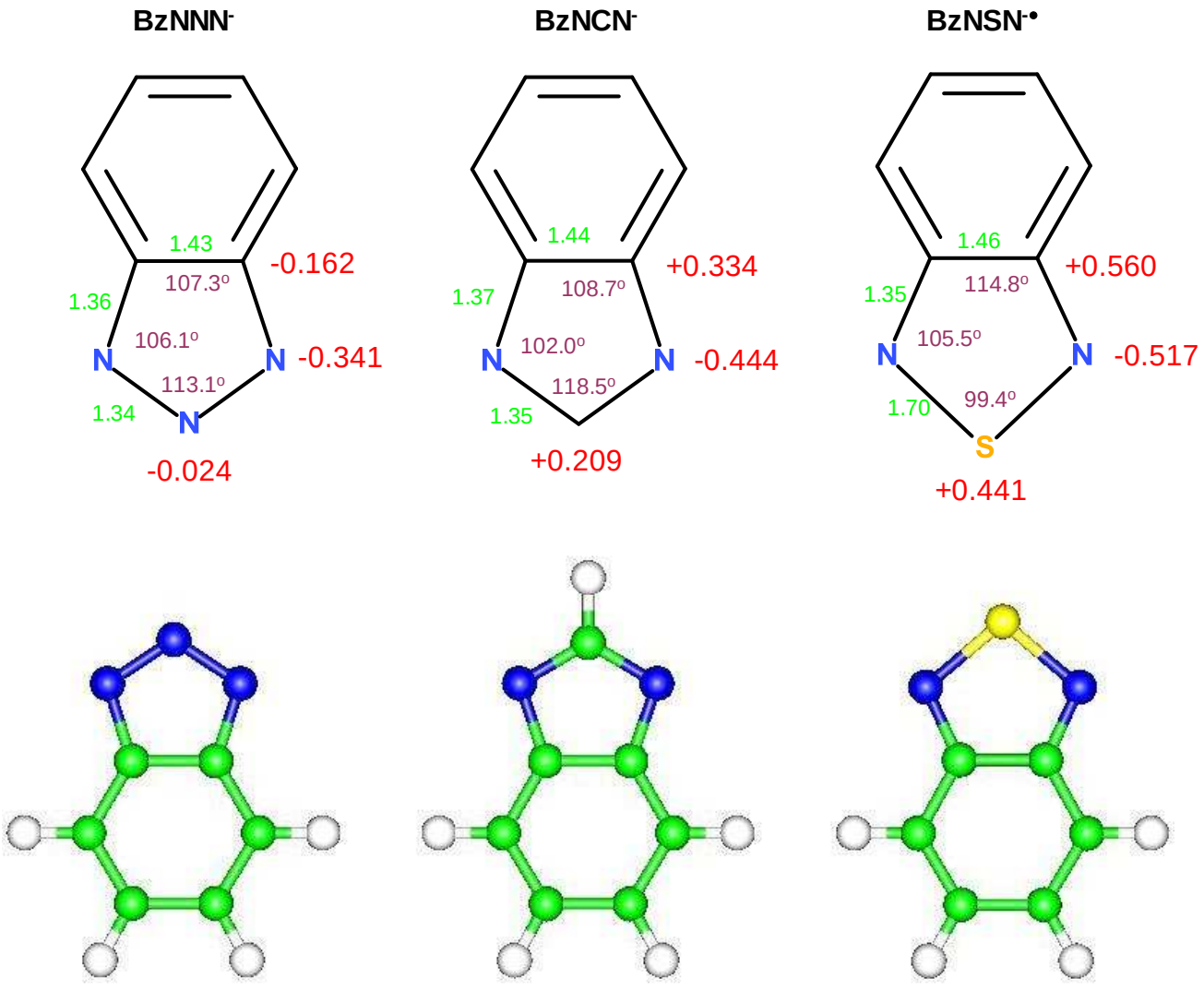

Section S1. Syntheses of anolyte mimics (Schemes 2 and S1) and Li^+ $BzNSN^{-\bullet}$.

The synthesis of $BzNNN^-$ compounds is analogous to the synthesis of $BzNCN^-$ compounds.

Lithium benzo[*d*]imidazolide (Li BzNCN). 1*H*-benzo[*d*]imidazole (14.17 g, 120 mmol) was dissolved in 200 ml aqueous tetrahydrofuran (1:1, v/v), followed by the addition of lithium hydroxide monohydrate (5.03 g, 120 mmol). The reaction mixture was vigorously stirred at room temperature for 2 h before the solvent was removed *in vacuo*. Then, to the crude product 200 ml of acetonitrile was added and the resulting suspension was filtered to remove the solid residue. The filtrate was reduced in vacuum to obtain the product (12.1 g, 80%).
^{1}H NMR (300 MHz, CD_3CN) δ 8.02 (s, 1H), 7.63-7.60 (m, 2H), 7.24-7.21 (m, 2H). ^{13}C NMR (75 MHz, CD_3CN) δ 143.0, 139.0, 121.7, 117.4, 115.5. ^{7}Li NMR (119 MHz, CD_3CN) δ 0.38.

Tetrabutylammonium benzo[*d*]imidazolide (N_{4444} BzNCN). 1*H*-benzo[*d*]imidazole (9.85 g, 83 mmol) was dissolved in 150 ml mixed solvent of acetonitrile and deionized water (1:1, v/v), followed by the addition of 54.6 ml of tetrabutylammonium hydroxide aqueous solution (~40% in water). The reaction mixture was vigorously stirred at room temperature for 2 hours before the solvent was removed *in vacuo* to obtain the product (23.5 g, 78%).
^{1}H NMR (300 MHz, CD_3CN) δ 7.84 (s, 1H), 7.48-7.45 (m, 2H), 6.89-6.86 (m, 2H), 3.04 (t, J = 9 Hz, 8H), 1.56 (q, J = 9 Hz, 8H), 1.33 (sextet, J = 7.5 Hz, 8H), 0.95 (t, J = 7.5Hz, 12H). ^{13}C NMR (75 MHz, CD_3CN) δ 150.1, 144.7, 117.8, 117.4, 115.9, 58.1, 23.3, 19.3, 12.9.

Lithium 2,1,3-benzothiazolide ($Li^+BzNSN^{-\bullet}$). In this synthesis, lithium was reacted with naphthalene in tetrahydrofuran (THF) to obtain lithium naphthalenide. The latter solution was reacted with BzNSN to reduce it to red $Li^+BzNSN^{-\bullet}$, which can be separated as a brown residue and washed with THF to remove naphthalene. The resulting solvate compound contains 2.0-2.5 molecules of THF per Li^+ ion that is replaced in the coordination sphere of this ion in the acetonitrile in solution. The direct reduction of BzNSN with metallic lithium was inefficient due to the formation of insoluble reaction products on the surface. Such reaction, however, is facile with metallic Na and K, but only in dilute solution (10 mM).

The synthesis was performed in a glovebox and all experimental apparatus were oven-dried at 100 ^{o}C overnight before usage. 25.3 g (197 mmol) of naphthalene was dissolved in 200 ml of anhydrous THF dried over molecular sieves, followed by adding 1.38 g (197 mmol) lithium foil in small portions. Upon addition of Li, the reaction mixture turned dark green almost immediately and was vigorously stirred for 30 min at room temperature. Then, 26.9 g (197 mmol) of BzNSN was added to the solution above in portions, resulting in a dark purple-reddish color (CAUTION! Exothermic reaction). The reaction mixture was allowed to stir for 1 h before precipitating the salt by addition of dry pentane (500 ml). The solid residue was collected on a porous glass frit. This crude product was dissolved in a minimum amount of THF and precipitated again by addition of pentane for complete removal of naphthalene, which is a reaction byproduct. The precipitate was dried in a vacuum oven at 25 ^{o}C overnight to give final product as a brown-red solid (3.04 g, 10.8%). When dissolved in acetonitrile, this material yields dark red solutions with the absorption and EPR spectra that are similar to the electrochemically generated $BzNSN^{-\bullet}$ in acetonitrile. To establish the composition of this solid and the concentration of the radical anion, aliquots of the acetonitrile solutions were mixed 1:1 v/v with 2-propanol or dimethylsulfoxide and the resulting mixtures were

stirred in air for 1 min to destroy the radical anion by oxidation with the oxygen. An aliquot of this "quenched" solution was diluted 1:10 v/v with $CDCl_3$, and ^1H NMR spectroscopy was used to compare the integrals over the aromatic protons and THF protons with the co-solvent protons. No resonances from the naphthalene were observed, suggesting its complete removal; however, during this "quenching" 15-25% of BzNSN converted to another product with the set of two *dd* protons (*J*=6.3 and 3.3 Hz) as the parent compound, suggesting the NSN ring opening. We have tallied this secondary product into our estimates of the radical anion concentration in the solution.

Section S2. NMR measurements: diffusion.

Program *ledbpgp2s* from DOSY suite was used for the stimulated echo measurements with longitudinal eddy-current delays, bipolar gradient pulses for diffusion and two spoil gradients. [1, 2] For all nuclei, the gradient recovery delay (D16) was 0.2 ms, the eddy current delay (D21) was 5 ms, and the spoil gradient pulse (P19) was 0.6 ms. The typical settings for other relevant parameters were as specified in the table below

parameter	**Bruker parameter**	**time unit**	**magnetic nucleus**				
			^{1}H	**^{19}F**	**^{7}Li**	**^{11}B**	**^{13}C**
acquisition time	AQ	s	2.3	3	5	5	11
relaxation delay	D1	s	3		10		
Δ	D20	ms	60		300		
δ/2	P30	ms	1.0		1.0	1.5	1.5

Section S3. Viscosity measurements.

Viscosity is measured using an m-VROC viscometer with B05 chip from RheoSense, Inc. An operator specified flow rate is applied via a syringe pump into a rectangular micro-channel (dimensions 51.1 μm x 2 mm x 1.5 cm). Three sensors along the length of the slot measure the pressure drop across the channel. The pressure drop ΔP can be related to the intrinsic shear stress through geometric factors as

$$\tau = -\frac{\Delta P}{2L}\frac{wh}{w+h} \quad \text{(S1)}$$

Similarly, the apparent shear rate of the fluid through the channel is related to the applied flow rate of the Newtonian fluid solution through geometric factors as

$$\gamma = 6Q/wh^2 \quad \text{(S2)}$$

Corrections can be made to compute the shear rate as necessary for non-Newtonian fluids. The viscosity η is then calculated from

$$\eta = \tau/\gamma \quad \text{(S3)}$$

Measurements are bounded by the maximum pressure drop per unit length of 4,000 Pa/mm and the minimum measurable pressure drop per unit length of 40 Pa/mm.

Section S4. QSPR analysis.

The intent of QSPR analysis is to correlate measured molecular properties with a set of structural descriptors; the relationships established for a limited training set can then be used for predicting properties for molecules that are not included in this set. We first describe how the descriptor set was obtained, then how multivariate multiple linear regression (MMLR) proceeded, and finally briefly describe the solution found. The complete list of descriptors and this solution are given in the Excel worksheet placed in the Supplement.

S4.1. Descriptors. The Python based RDKit [3] was used to generate chemical structures of the ions using MMFF94 force field. These structures were subsequently optimized using PM6 semiempirical method from Gussian 91 and the coordinates fed into Mordred descriptor calculator, which is another Python based program [4] that works together with RDKit. The Excel worksheet in the Supplement lists the Internet addresses for the software and the relevant documentation. This software generates 1200+ descriptors for each cation and anion, some of which depend only on the bonding structure (2D descriptors) while other depend on the three dimensional structure (3D descriptors). Each salt included two independent sets of descriptors, one for the cation and another for the anion. Several parameters including molecular radii and volumes, weighted inertia ellipsoids, etc. were calculated using Gaussian outputs and added to the descriptor lists generated by Mordred. We also added several *ad hoc* descriptors, such as the counts of cyanide groups as well as *Hato, Chi4c,* and *Smax14* descriptors introduced in ref. [5] specifically for anions in ionic liquids. Many of these descriptors are tightly correlated with each other, so the majority of these descriptors can be excluded by retaining only the ones that have correlation coefficients $\rho<0.9$ with each other. Interquartile range test was used to exclude descriptors that are excessively clustered for certain compounds. These two tests excluded all but 278 descriptors.

S4.2. MMLR analysis. In MMLR, the experimental variables/measurements $\boldsymbol{Y}=\{y_{ik}\}$ (i=1,…N_y variables for k=1,…N measurements) are linearly correlated with the explanatory variables $\boldsymbol{X}=\{x_{jk}\}$ (j=1,…N_x variables for k=1,…N measurements) that include both the molecular descriptors and environmental parameters, such as temperature, pressure, or concentration:

$$\boldsymbol{Y} = \boldsymbol{X}\,\boldsymbol{\beta} + \boldsymbol{\varepsilon} \qquad \text{(S4)}$$

where $\boldsymbol{\beta}$ is a coefficients matrix to be determined and $\boldsymbol{\varepsilon}$ is the residuals matrix, whose norm $\|\boldsymbol{\varepsilon}\|$ is minimized using the calculus of variations. Eq. S4 relates to the standard form variables, in which the means of N measurements are subtracted from each $\boldsymbol{x}$ and $\boldsymbol{y}$ variable and the resulting differences are normalized by the standard deviation for the corresponding variables. It is easy to show that the optimum matrix $\boldsymbol{\beta}$ is given by [6]

$$\boldsymbol{\beta} = \mathbf{S}_{xx}^{-1}\mathbf{S}_{yx} \qquad \text{(S5)}$$

where $\mathbf{S}_{xx}=\boldsymbol{X}^t\boldsymbol{X}$ is the matrix of covariations, $\mathbf{S}_{yx}=\boldsymbol{X}^t\boldsymbol{Y}$, and the solution $\hat{\boldsymbol{Y}}$ is given by

$$\hat{\boldsymbol{Y}}=\boldsymbol{X}\,\boldsymbol{\beta}\,, \qquad \text{(S6)}$$

so that $\boldsymbol{\varepsilon}=\boldsymbol{Y}-\hat{\boldsymbol{Y}}$. The coefficient of determination R^2, which is the measure of multivariate association for univariate multiple linear regression, cannot be uniquely defined for multivariate regression, [6] and we used the Wilks measure (that is also known as the Hotelling-Cramer measure) given by

$$R^2=det[\mathbf{S}_{\varepsilon\varepsilon}]/det[\mathrm{S}_{yy}]=det[\mathbf{S}_{yy}-\mathbf{S}_{\hat{y}\hat{y}}]/det[\mathbf{S}_{yy}] \qquad \text{(S7)}$$

where $\mathbf{S}_{\varepsilon\varepsilon}=\boldsymbol{\varepsilon}^t\boldsymbol{\varepsilon}$ and $\mathbf{S}_{\hat{y}\hat{y}}=\hat{\boldsymbol{Y}}^t\hat{\boldsymbol{Y}}$.

It should be noted that many of the explanatory variables in $\boldsymbol{X}$ are correlated with each other, so the rank of $\mathbf{S}_{xx}$ can be much smaller than N_x. The art of QSPR is in finding the smallest subset of explanatory variables that accounts for most of variation in the training set. This is typically achieved using ridge, Lasso, [7] or elastic net regularization, [8] but these methods proved ineffective for smaller sets. Instead we used a genetic optimization algorithm for selecting the "minimal" descriptor subset which was introduced in ref. [9]; our implementation of the algorithm is quite different from this pervious study.

Briefly, multiple subsets χ of $m<N_x$ variables ("chromosomes", with each explanatory variable being a "gene") are generated at random and eqs. S5 and S6 are solved for each subset. Parameter $(1-R^2)$ given by eq. S7 for each "chromosome" serves as the measure of "fitness". At each iteration, 50 "chromosomes" are sorted by their fitness and 10 most fit "chromosomes" are selected at random according to the precedence of their fitness. Two "mutations" (random substitutions of the "genes") are introduced per "chromosome". Fragments of these chromosomes are pairwise interchanged in similarity to crossing over in the real chromosomes. As the fragments are exchanged, some "genes" become duplicated, which is equivalent to reducing the size m of subset χ. These variations are introduced at each generation, as the population of "chromosomes" evolves searching for the global minimum. Typically, $(0.1\text{-}2)\times10^3$ iterations were sufficient to find the optimal subset χ for a given m in a matter of minutes. For this optimal subset χ the rank r_χ for the covariance matrix $\mathbf{S}\chi\chi$ is calculated and if $r_\chi < m$, m is reduced accordingly and the procedure is repeated.

For measurements that depend on environmental parameters, the coefficients β before these parameters can themselves be dependent on molecular descriptors. Furthermore, for salts one can expect that some coefficients β are dependent on correlations between the molecular descriptors for anions and cations. To address these concerns, the following protocol was used.

For the given set of m_e environmental parameters, the number m_d of the descriptors was fixed and genetic optimization for $m=m_e+m_d$ variables was used to find the best subset χ (the "linear set"). This linear set was then used for quadratic expansion: to this set a new χ x χ set (the direct product of χ by itself) was added to introduce quadratic terms. This combined set was parsed using the same criteria which we used to reduce the original descriptor set, and the genetic algorithm optimization was applied once again to a subset of $m=2m_e+m_d$ variables, searching for the global minimum in this "quadratic set." In this way, the linear space is expanded and fit quality is improved without introducing new descriptors. We stress that the selected sets are not unique, as there is significant correlation between the descriptors even after parsing the descriptor sets using our criteria. Such correlations, however, do not affect the predictive ability of the resulting subsets.

S4.3. MMLR results. As y-variables for MMLR, we selected the density and ion diffusivities (D_+ and D_-) of salt solutions in CD_3CN and assumed (as suggested by our LiTFSI results in section 1) that these variables linearly depend on the molar concentration c of the salt and $c^{1/2}$ ($m_e=2$). As

input we had a set of 53x3 measurements for 45 salts (see the Excel worksheet in the Supplement). Using our procedure, we first found a linear subset of m_d=8 descriptors, from which a quadratic set of 27 variables was constructed (after parsing 8x8 additional variables). From this quadratic set we chose an optimum subset of 18 variables, which are given in the Excel worksheet along with the fit and the residuals. This fit is graphically summarized in Figure S8, with the individual coefficients of determination r^2 given for each *y*-variable. Our "minimal" set of eight descriptors, which included three cation descriptors and five anion descriptors was sufficient to fit the entire set with R^2=0.9998 and the root mean square error of 0.25. The linear terms of the quadratic set included two cation and three anion descriptors and ten quadratic terms that included six cross terms for anion and cation descriptors, two cross terms for anion descriptors and *c*, and one cross term for cation descriptor and $c^{1/2}$.

Most of these descriptors were 2D descriptors that included Moreau-Broto autocorrelations (also known as autocorrelations of topological structure), a Moran coefficient, and a Burden eigenvalue, [10] which do not have intuitive meanings. Two descriptors, however, have a clear intuitive meaning. For cations, one of the selected descriptors was r_+^{-1}, where r_+ is the molecular radius estimated from the semiempirical calculation. The proportionality of D_+ with r_+^{-1} is suggested by the Stokes-Einstein relation, so the cation size plays an important role in determining the cation diffusivity even in concentrated solutions. Two other topological descriptors characterize the distribution of van der Waals radii and electronegativity across the cation. For anions, one of the major descriptors was the number of cyano groups in the anion, which strongly correlates with the higher D_- for the outliers in Table 5. Four other descriptors were topological, and characterized the distribution of the atomic ionic potentials, numbers and van der Waals volumes across the anions. These descriptors can be calculated for other cations and anions (including charged ROMs) and inserted into eq. S6 to predict the concentration dependence of density and ionic diffusivity for salts in CD_3CN. The coefficient matrix β for this extrapolation is given in the Excel sheet in the Supplement.

Table S2. Cumulative Properties of Selected Salts in Acetonitrile.

cation	anion	conc., M	density, g/cm^3	x 10^{-6} cm^2/s			Λ_{est} (1 M) S·cm^2/mol	σ_{est} mS/cm
				D_+	D_-	D		
Li	BF_4	1.14	0.959	6.07	6.55	12.62	48.06	54.70
Li	PF_6	0.53	0.992	6.57	9.35	15.92	60.63	31.87
Li	CF_3CO_2	1.01	0.925	5.15	5.32	10.47	39.87	40.09
Li	TfO	1.00	0.992	5.54	5.83	11.37	43.30	43.23
Li	DFOB	0.91	0.938	6.39	7.90	14.29	54.42	49.42
Li	BOB	0.73	0.957	6.61	7.06	13.67	52.06	37.99
Li	FSI	0.92	0.998	6.75	8.25	15.00	57.13	52.59
Li	TFSI	0.89	1.076	7.89	7.95	15.84	60.32	53.70
Li	BETI	0.88	1.114	6.44	5.23	11.67	44.44	39.31
Li	CTf_3	1.01	1.169	6.10	5.93	12.03	45.81	46.32
Li	TDI	0.85	0.968	7.46	6.32	13.78	52.48	44.75
N_{1111}	BF_4	0.10	0.927	17.50	13.15	30.65	116.78	11.68
N_{2222}	BF_4	0.81	0.909	10.54	8.24	18.78	71.55	58.23
N_{3333}	BF_4	0.81	0.946	7.91	9.29	17.20	65.53	53.35
N_{4444}	BF_4	0.81	0.959	6.31	8.42	14.73	56.11	45.50
C_4mim	BF_4	0.86	0.964	8.91	8.50	17.41	66.34	56.97
MeImBz	BF_4	0.93	0.960	7.67	7.79	15.46	58.90	55.05
4MePyBu	BF_4	0.99	0.981	8.45	8.15	16.60	63.25	62.89
N_{1111}	PF_6	0.12	0.887	17.81	16.45	34.26	130.53	15.66
N_{2222}	PF_6	0.97	0.982	9.62	9.92	19.54	74.45	72.54
N_{4444}	PF_6	0.77	0.945	6.34	7.56	15.92	60.63	46.47
C_4mim	PF_6	1.02	0.990	8.98	8.20	17.18	65.45	66.61
MeImBz	PF_6	0.97	1.048	7.80	7.75	15.36	58.52	56.63
PyBz	PF_6	0.74	1.032	8.29	7.94	16.23	61.84	45.76
4MePyBu	PF_6	0.95	1.015	8.52	8.34	16.86	64.24	60.75
4CNPyBz	PF_6	0.86	1.071	5.41	6.19	11.60	44.19	38.00
di(MeO)Im	PF_6	0.78	1.035	8.93	8.78	17.71	67.49	52.64
N_{1111}	TFSI	1.07	1.055	10.84	8.44	19.28	73.46	78.78
HN_{222}	TFSI	1.02	1.056	9.23	6.58	15.81	60.24	61.15
N_{2222}	TFSI	1.06	1.068	8.61	7.97	16.58	63.17	66.67
NBu_4	TFSI	0.90	1.058	4.89	5.14	10.03	38.21	34.48
S_{222}	TFSI	1.03	1.059	9.97	7.31	17.28	65.84	67.78
$P_{1,4}$	TFSI	1.00	1.030	8.02	5.97	13.99	53.31	53.47
C_2mim	TFSI	1.06	1.055	9.05	6.26	15.31	58.33	62.10
PyBz	TFSI	1.02	1.096	6.89	5.36	12.25	46.68	47.52

4CNPyBz	TFSI	0.96	1.097	5.38	5.09	10.47	39.88	38.22
MeImBz	TFSI	1.09	1.090	5.97	6.29	12.26	46.71	51.01
PyEt	TFSI	1.17	1.104	8.93	5.31	14.24	54.25	63.59
$N_{112}(C_2H_4OMe)$	$B(CN)_4$	1.14	0.941	8.62	10.30	18.92	72.07	82.16
$P_{1,4}$	$B(CN)_4$	1.06	0.987	10.07	12.20	22.27	84.87	90.05
C_2mim	$B(CN)_4$	1.10	0.934	10.27	12.20	22.47	85.61	94.26
PyOc	$B(CN)_4$	0.99	0.927	7.03	13.00	20.03	76.31	75.76
$P_{1,4}$	DCA	0.95	0.933	9.00	15.00	24.00	91.43	86.78
C_2mim	DCA	1.12	0.957	10.12	18.00	28.12	107.14	119.99

Table S3. Cumulative Properties of Acetonitrile Soluble Salts (Descending Order in σ_{est}).

cation	anion	conc., M	density, g/cm^3	x 10^{-6} cm^2/s			σ_{est}, mS/cm	Λ_{est}, S·cm^2/mol at 1 M	Λ_{est} % of LiTFSI
				D_+	D_-	D			
C_2mim	DCA	1.12	0.957	10.12	18.00	28.12	119.99	107.14	223
C_2mim	$B(CN)_4$	1.10	0.934	10.27	12.20	22.47	94.26	85.61	176
$P_{1,4}$	B(CN)4	1.06	0.987	10.07	12.20	22.27	90.05	84.87	168
$P_{1,4}$	DCA	0.95	0.933	9.00	15.00	24.00	86.78	91.43	162
$N_{112}(C_2H_4OMe)$	$B(CN)_4$	1.14	0.941	8.62	10.30	18.92	82.16	72.07	153
N_{1111}	TFSI	1.07	1.055	10.84	8.44	19.28	78.78	73.46	147
PyOc	$B(CN)_4$	0.99	0.927	7.03	13.00	20.03	75.76	76.31	141
N_{2222}	PF_6	0.97	0.982	9.62	9.92	19.54	72.54	74.45	135
S_{222}	TFSI	1.03	1.059	9.97	7.31	17.28	67.78	65.84	126
N_{2222}	TFSI	1.06	1.068	8.61	7.97	16.58	66.67	63.17	124
C_4mim	PF6	1.02	0.990	8.98	8.20	17.18	66.61	65.45	124
PyEt	TFSI	1.17	1.104	8.93	5.31	14.24	63.59	54.25	118
4MePyBu	BF_4	0.99	0.981	8.45	8.15	16.60	62.89	63.25	117
C_2mim	TFSI	1.06	1.055	9.05	6.26	15.31	62.10	58.33	116
HN_{222}	TFSI	1.02	1.056	9.23	6.58	15.81	61.15	60.24	114
4MePyBu	PF_6	0.95	1.015	8.52	8.34	16.86	60.75	64.24	113
N_{2222}	BF_4	0.81	0.909	10.54	8.24	18.78	58.23	71.55	108
MeImBz	PF_6	0.97	1.048	7.80	7.75	16.04	59.13	61.11	110
C_4mim	BF_4	0.86	0.964	8.91	8.50	17.41	56.97	66.34	106
MeImBz	BF_4	0.93	0.960	7.67	7.79	15.46	55.05	58.90	103
Li	BF_4	1.14	0.959	6.07	6.55	12.62	54.70	48.06	102
Li	TFSI	0.89	1.076	7.89	7.95	15.84	53.70	60.32	100
$P_{1,4}$	TFSI	1.00	1.030	8.02	5.97	13.99	53.47	53.31	100
N_{3333}	BF_4	0.81	0.946	7.91	9.29	17.20	53.35	65.53	99
di(MeO)Im	PF_6	0.78	1.035	8.93	8.78	17.71	52.64	67.49	98
Li	FSI	0.92	0.998	6.75	8.25	15.00	52.59	57.13	98
MeImBz	TFSI	1.09	1.090	5.97	6.29	12.26	51.01	46.71	95
Li	DFOB	0.91	0.938	6.39	7.90	14.29	49.42	54.42	92

Continued.

cation	anion	conc., M	density, g/cm^3	D_+	D_-	D	σ_{est}, mS/cm	Λ_{est}, S·cm^2/mol at 1 M	Λ_{est} % LiTFSI
PyBz	TFSI	1.02	1.096	6.89	5.36	12.25	47.52	46.68	88
N_{4444}	PF_6	0.77	0.945	6.34	7.56	15.92	46.47	60.63	87
Li	CTf_3	1.01	1.169	6.10	5.93	12.03	46.32	45.81	86
PyBz	PF_6	0.74	1.032	8.29	7.94	16.23	45.76	61.84	85
N_{4444}	BF4	0.81	0.959	6.31	8.42	14.73	45.50	56.11	85
Li	TDI	0.85	0.968	7.46	6.32	13.78	44.75	52.48	83
Li	TfO	1.00	0.992	5.54	5.83	11.37	43.23	43.30	80
Li	CF_3CO_2	1.01	0.925	5.15	5.32	10.47	40.09	39.87	75
Li	BETI	0.88	1.114	6.44	5.23	11.67	39.31	44.44	73
4CNPyBz	TFSI	0.96	1.097	5.38	5.09	10.47	38.22	39.88	71
4CNPyBz	PF_6	0.86	1.071	5.41	6.19	11.60	38.00	44.19	71
Li	BOB	0.73	0.957	6.61	7.06	13.67	37.99	52.06	71
N_{4444}	TFSI	0.90	1.058	4.89	5.14	10.03	34.48	38.21	64
Li	PF_6	0.53	0.992	6.57	9.35	15.92	31.87	60.63	59

Table S4. Viscosity change upon charging of electrolyte solutions containing A and C (1:1 equiv.) in acetonitrile (100%SOC, 5C rate). All viscosities are given in cP (21.2 ºC)

conc, mM	Supporting Electrolyte	Neutral electrolyte	Oxidized	Reduced	Change oxidized % [a]	Change reduced % [a]	Change oxidized σ [c]	Change reduced σ [c]
50	1 M LiTFSI	0.847±0.004 (0.46%)	0.872± 0.004 (0.50%)	0.849±0.012 (1.37%)	+2.93 (±0.96) [b]	0 (±1.83) [b]	3.0	0.1
50	1 M N_{4444} PF_6	0.911±0.003 (0.36%)	0.909± 0.004 (0.42%)	0.921±0.003 (0.32%)	-0.20 (±0.78) [b]	1.06 (±0.68) [b]	-0.3	1.6
50	0.5 M $LiPF_6$	0.659±0.006 (0.93%)	0.701± 0.009 (1.32%)	0.689±0.006 (0.89%)	+6.38 (±2.25) [b]	+4.63 (±1.82) [b]	2.8	2.5
50	1 M N_{4444} TFSI	0.534±0.006 (1.17%)	0.500± 0.008 (1.55%)	0.560±0.006 (1.08%)	-6.37 (±2.72) [b]	+5.03 (±2.25) [b]	-2.3	+2.2
250	1 M N_{4444} TFSI	0.646±0.012 (1.88%)	0.687± 0.025 (3.67%)	0.625±0.011 (1.69%)	+6.43	-3.15	1.2	-0.9

a) relative to the solution before electrolysis; b) confidence limits; c) change in the units of the standard deviation (σ) of the measurement. Three viscosity measurements per sample.

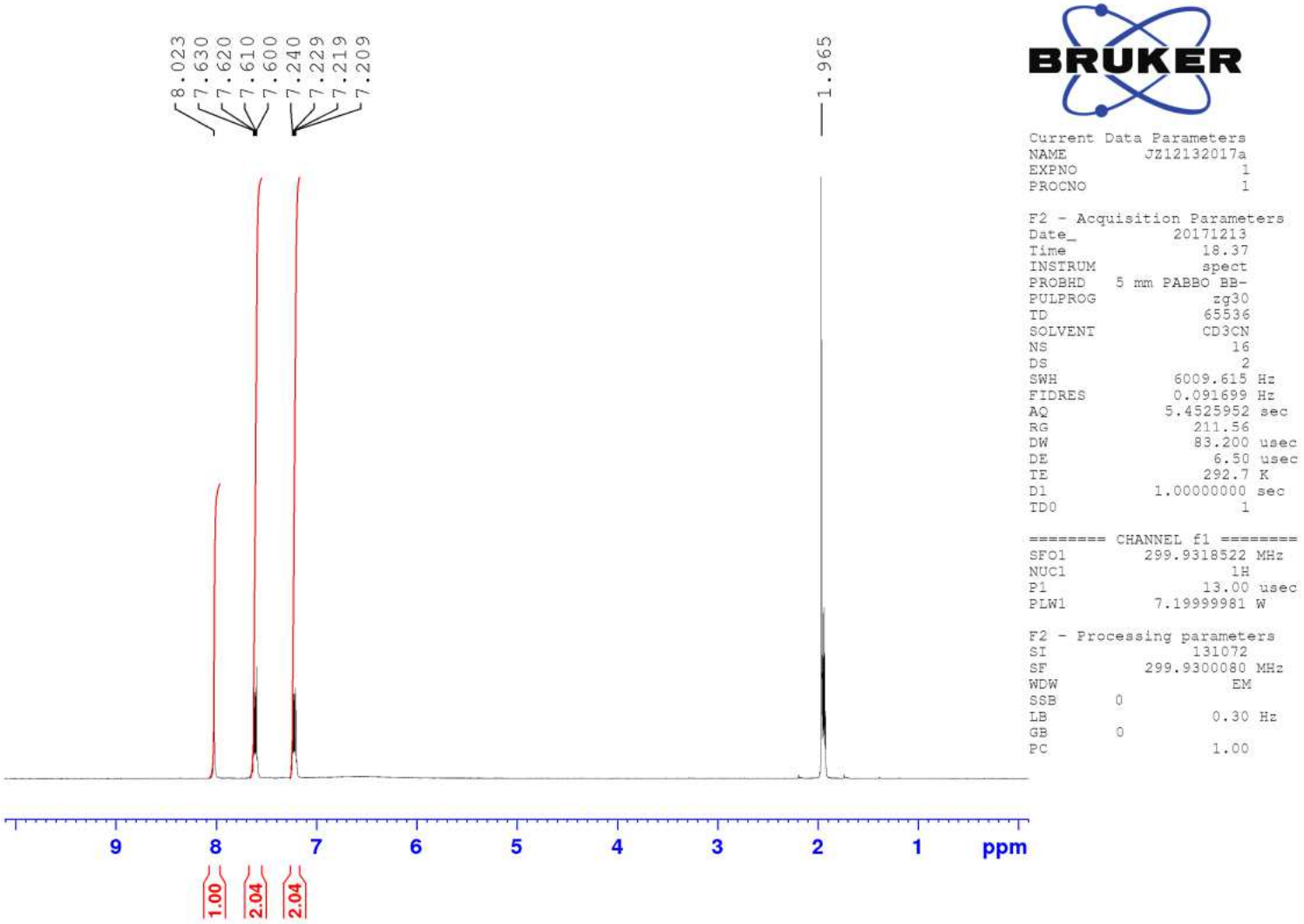

Figure S1. ^{1}H NMR spectrum of lithium benzo[*d*]imidazol-1-ide (LiBzNCN) in CD_3CN.

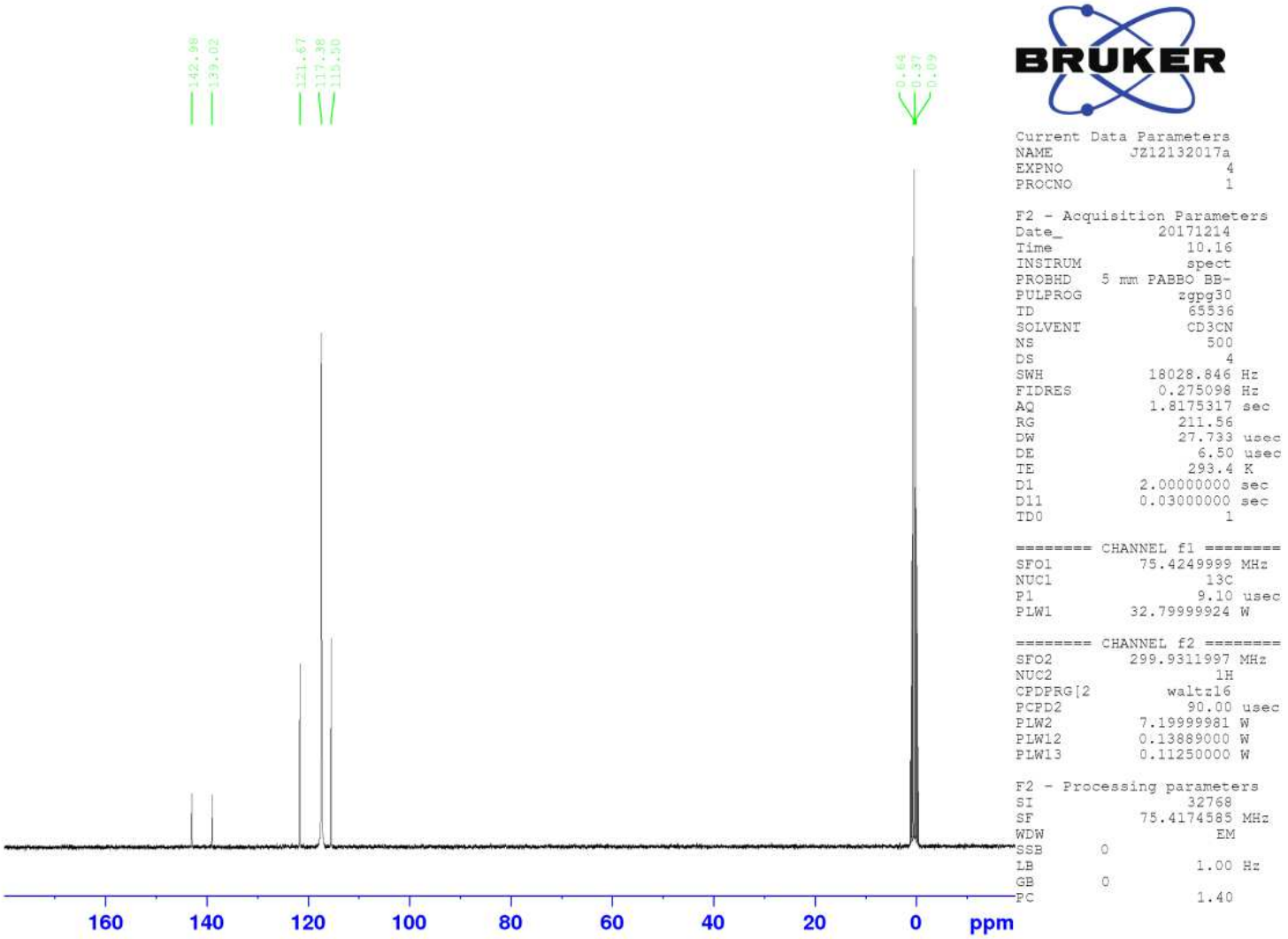

Figure S2. ^{13}C NMR spectrum of lithium benzo[*d*]imidazol-1-ide (LiBzNCN) in CD_3CN.

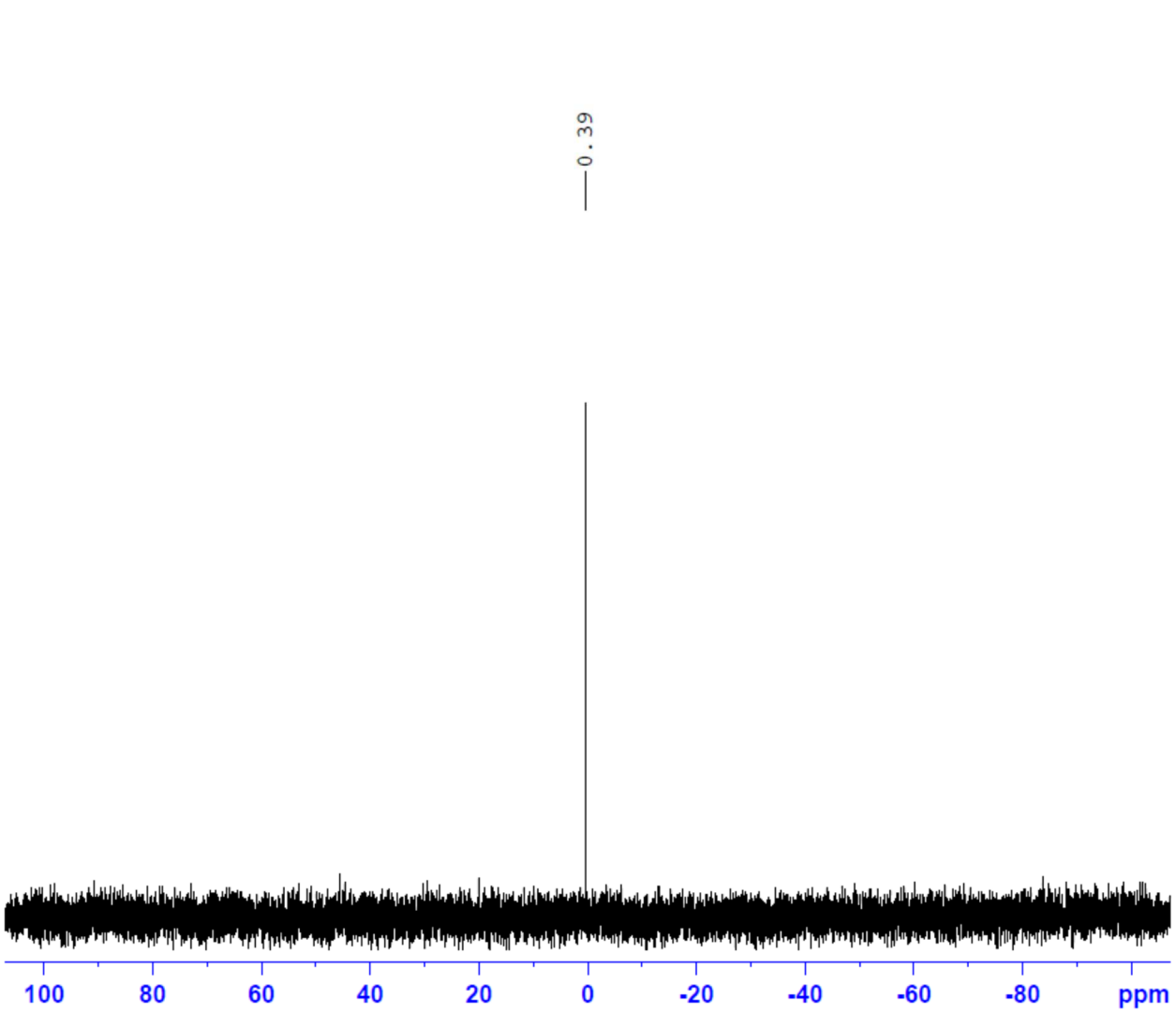


```
Current Data Parameters
NAME         JZ12132017a
EXPNO                  2
PROCNO                 1

F2 - Acquisition Parameters
Date_           20171213
Time               18.43
INSTRUM            spect
PROBHD   5 mm PABBO BB-
PULPROG               zg
TD                131072
SOLVENT            CD3CN
NS                    16
DS                     0
SWH            25000.000 Hz
FIDRES          0.190735 Hz
AQ             2.6214399 sec
RG                211.56
DW                20.000 usec
DE                 6.50 usec
TE                292.7 K
D1             5.00000000 sec
TD0                    1

======== CHANNEL f1 ========
SFO1         116.5641860 MHz
NUC1                7Li
P1                10.00 usec
PLW1         12.19999981 W

F2 - Processing parameters
SI                262144
SF           116.5641826 MHz
WDW                   EM
SSB       0
LB                 1.00 Hz
GB        0
PC                 1.00
```

Figure S3. ^{7}Li NMR spectrum of lithium benzo[*d*]imidazol-1-ide (LiBzNCN) in CD_3CN.

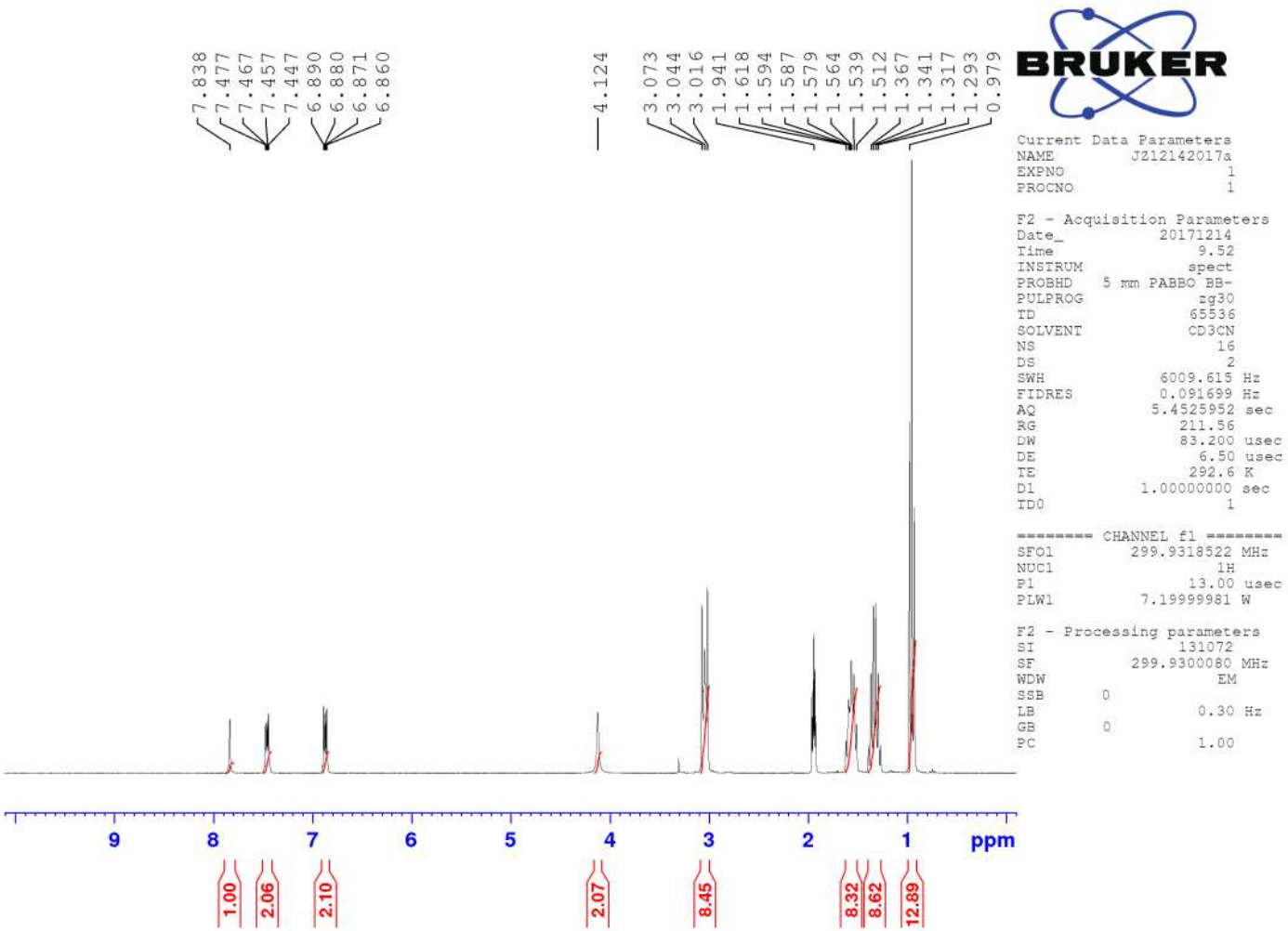

Figure S4. ^{1}H NMR spectrum of tetrabutylammonium benzo[*d*]imidazol-1-ide (N_{4444}BzNCN) in CD_3CN.

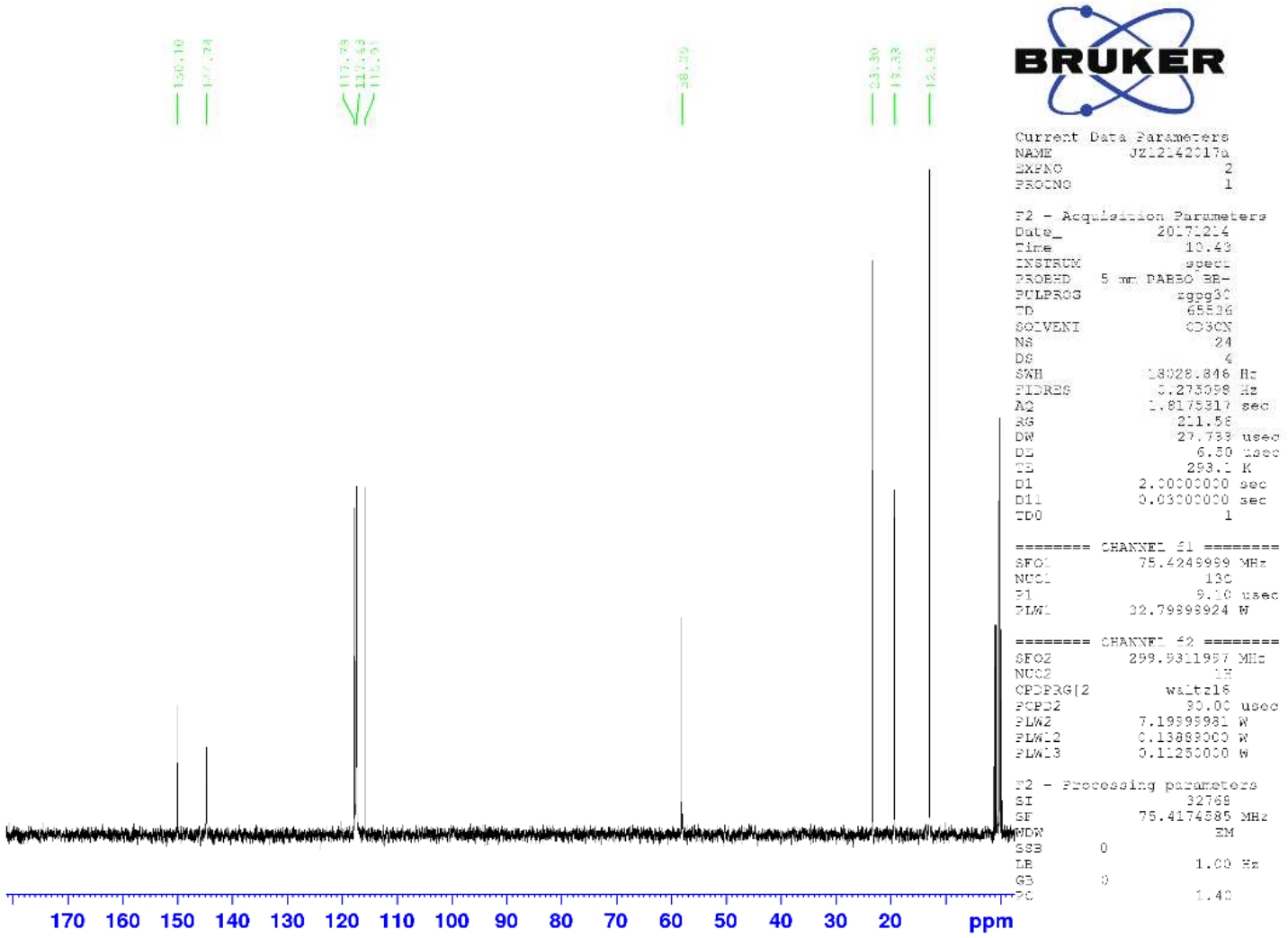

Figure S5. ^{13}C NMR spectrum of tetrabutylammonium benzo[*d*]imidazol-1-ide (N_{4444}BzNCN) in CD_3CN.

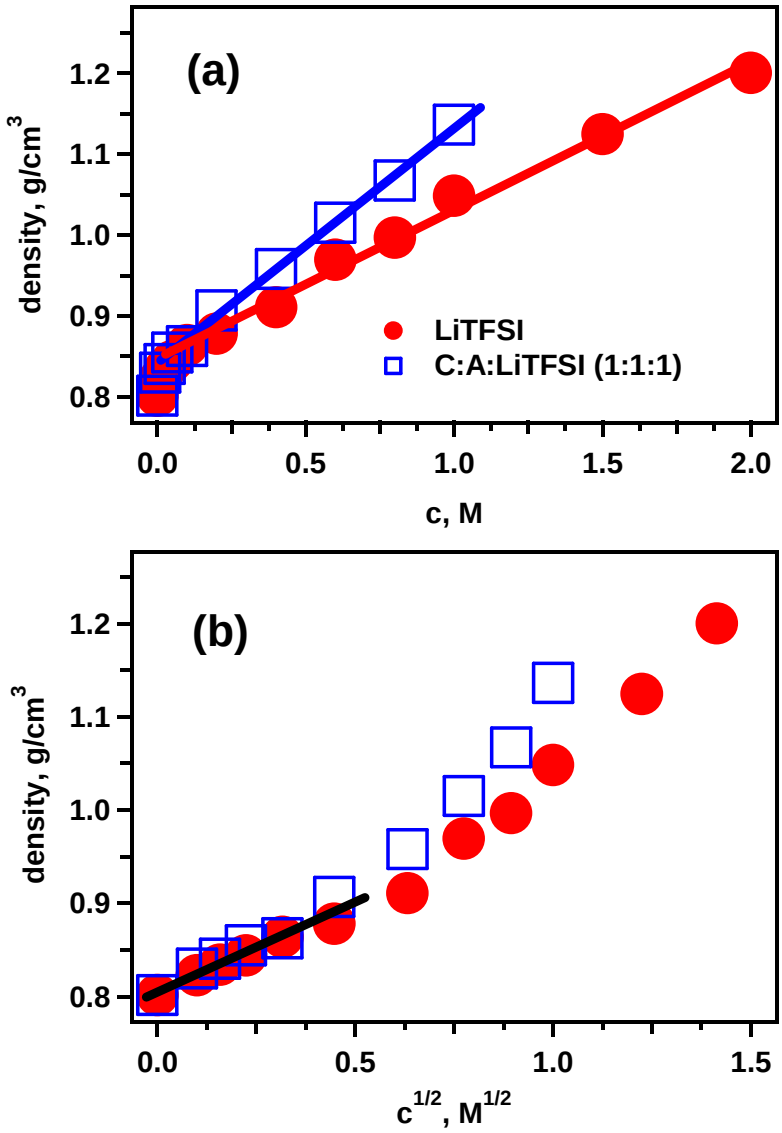

Figure S6. Densities of LiTFSI solutions (*filled circles*) at 25 °C as functions of LiTFSI concentration (c) plotted vs. c in panel a and $c^{1/2}$ in panel b. The open squares indicate the densities of solution containing 1:1:1 equiv. **C**, **A**, and LiTFSI. At low concentration (<0.2 M) the density increases as $c^{1/2}$, but at higher concentrations, it increases linearly with c. The bold lines are linear fits.

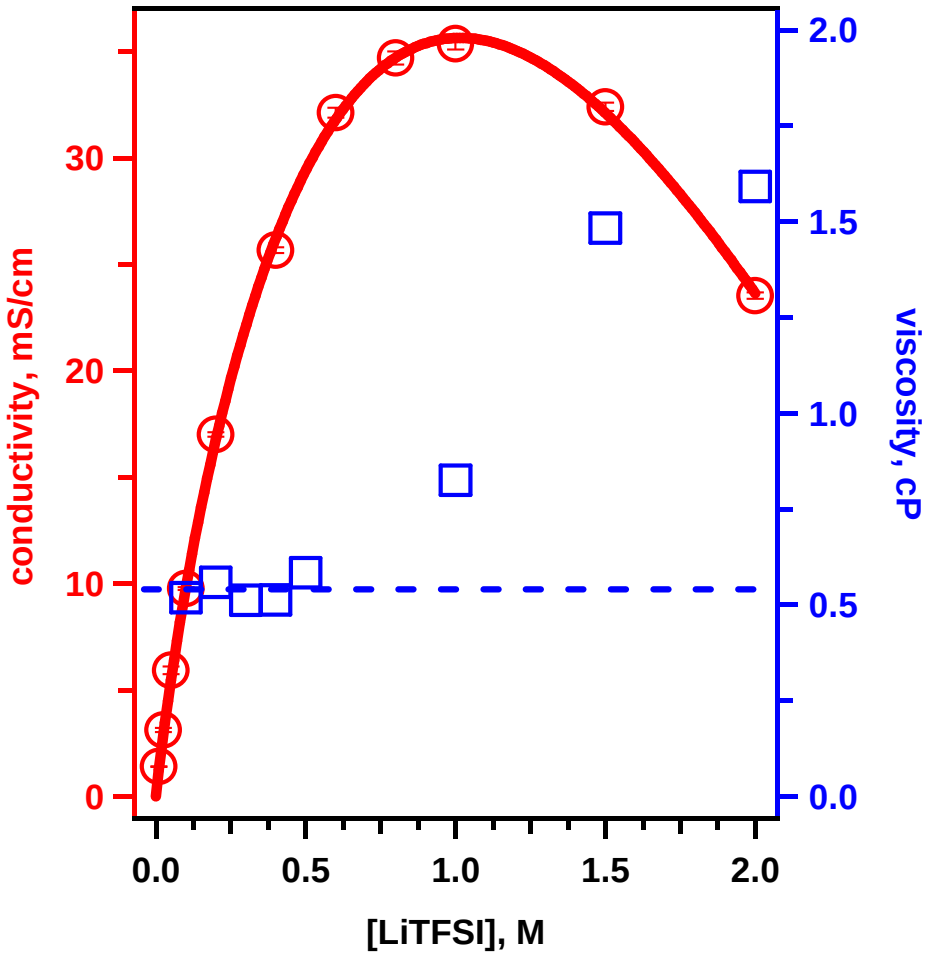

Figure S7. Conductivity σ (*to the left*) and viscosity η (*to the right*) of LiTFSI solutions in CH_3CN as a function of LiTFSI molarity at 25 °C. The bold lines are fit to eq. 8 corrected by the ion association.

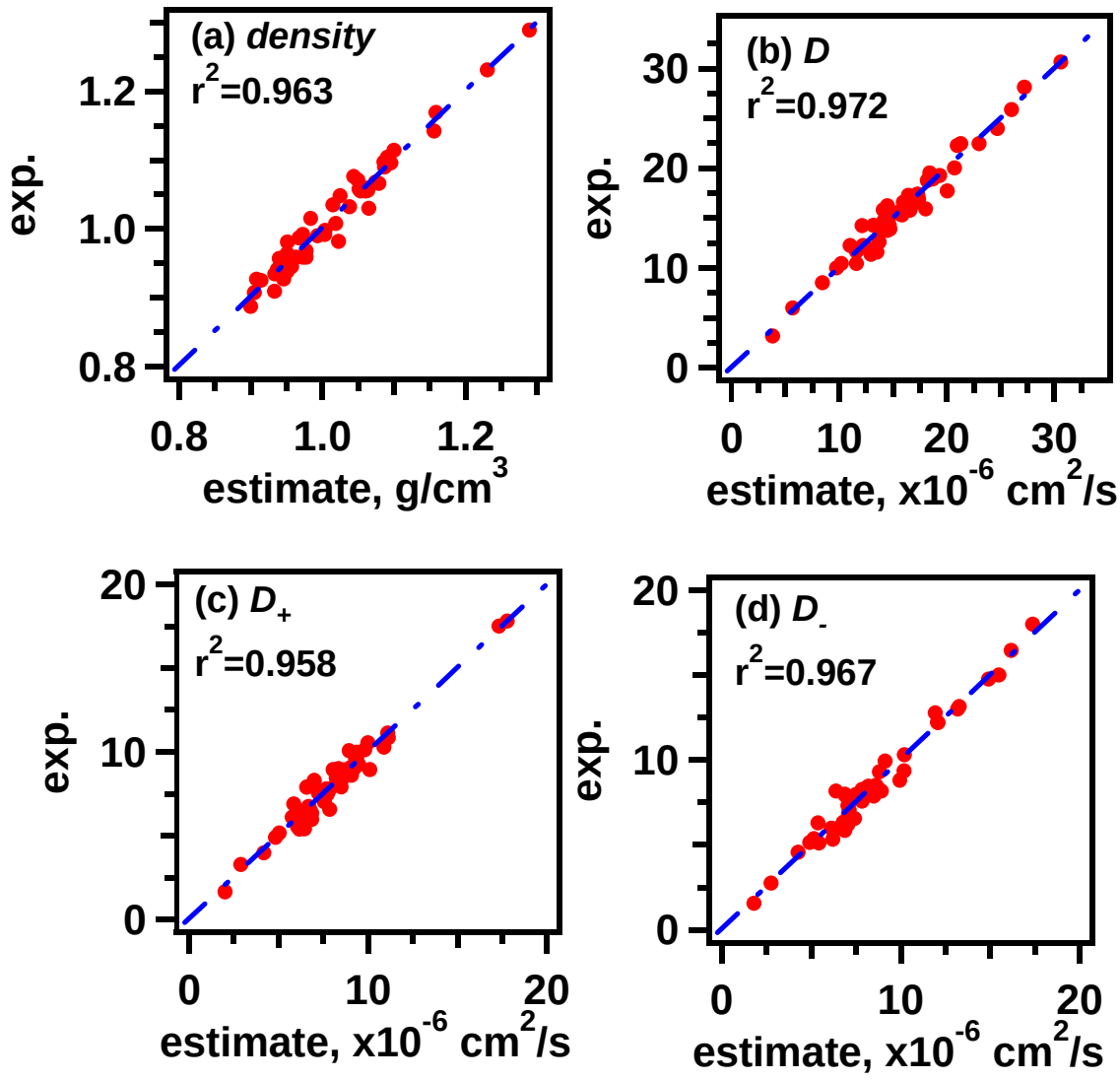

Figure S8. Results of QSPR analysis of a data set containing 53 measurements of (a) density and (b) joint ($D=D_+ + D_-$) and (c,d) ion ($D_\pm$) diffusivities for 45 salts in CD_3CN. These data were correlated using eight descriptors of ion properties. The coefficients of determination r^2 are indicated in the plots. See section S4 for more detail of this QSPR analysis.

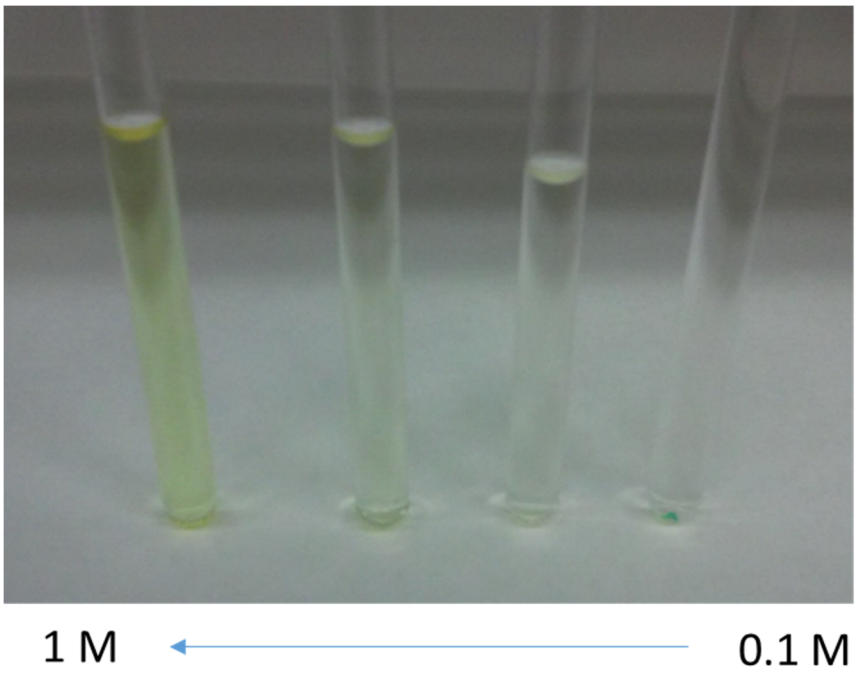

Figure S9. Formation of the yellow colored $\mathbf{C}^{\delta+}\mathbf{A}^{\delta-}$ donor-acceptor complex in 1:1 equiv. mixtures of the catholyte (**C**) and anolyte (**A**) molecules in acetonitrile (proportional dilution). See Scheme 1 for the structural formulas of these molecules.

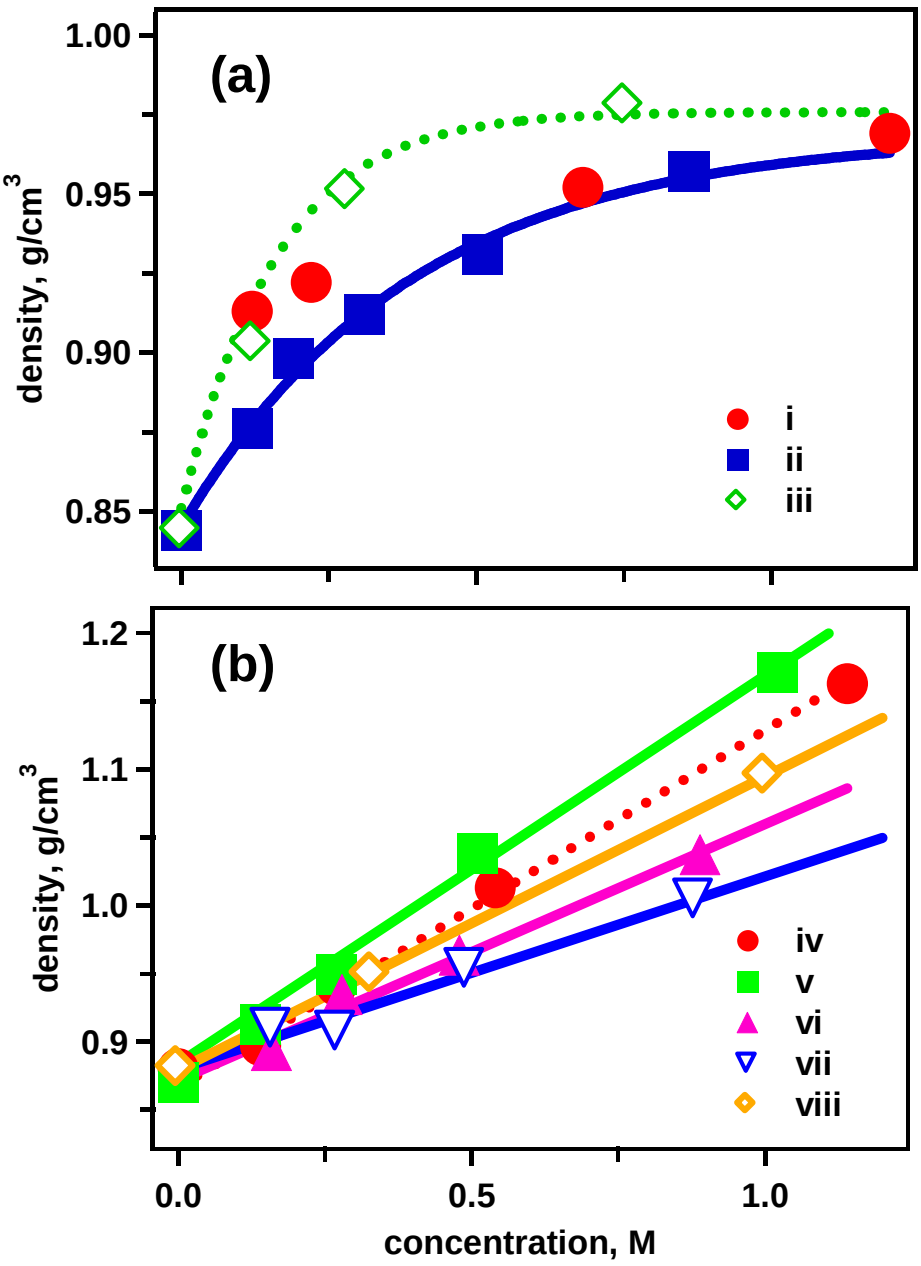

Figure S10. Solution density as a function of solute concentration (proportional dilution of all components) in CD_3CN at 25 °C. (a) Non-linear concentration dependencies for neutral solutes without salts, for (i) **A** alone, (ii) **C** alone, and (iii) 1:1 equiv. mixture of **A**:**C**. Nearly linear concentration dependencies with the salts, for (iv) 1:1:1.35 equiv. mixture of **A**:**C**:LiTFSI, (v) 1:1:1 equiv. **A**:**C**:LiTFSI, (vi) 1:1:1 equiv. **A**:**C**:$P_{1,4}$ DCA, (vii) 1:1:1 equiv. **A**:**C**:$P_{1,4}$ $B(CN)_4$, and (viii) 1:1:1 equiv. **A**:**C**:N_{4444} PF_6. The solid lines in panel a are guides to the eye; panel b shows the least squares linear fits.

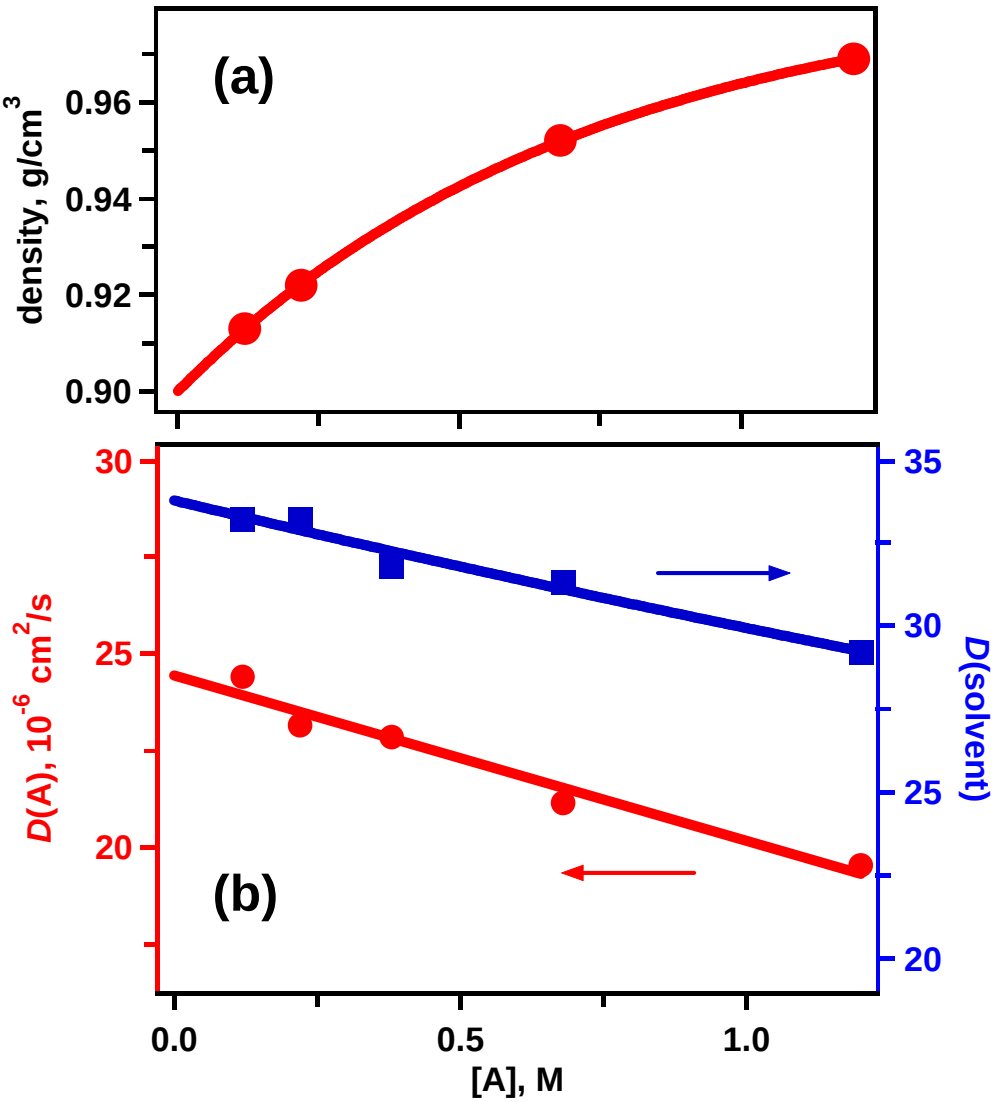

Figure S11. (a) Solution density and (b) coefficients for anolyte diffusion (*to the left*) and solvent self-diffusion (*to the right*) for solutions of **A** in in CD_3CN at 25 °C. Parabolic fit in panel a and linear fits in panel b are shown with the solid lines.

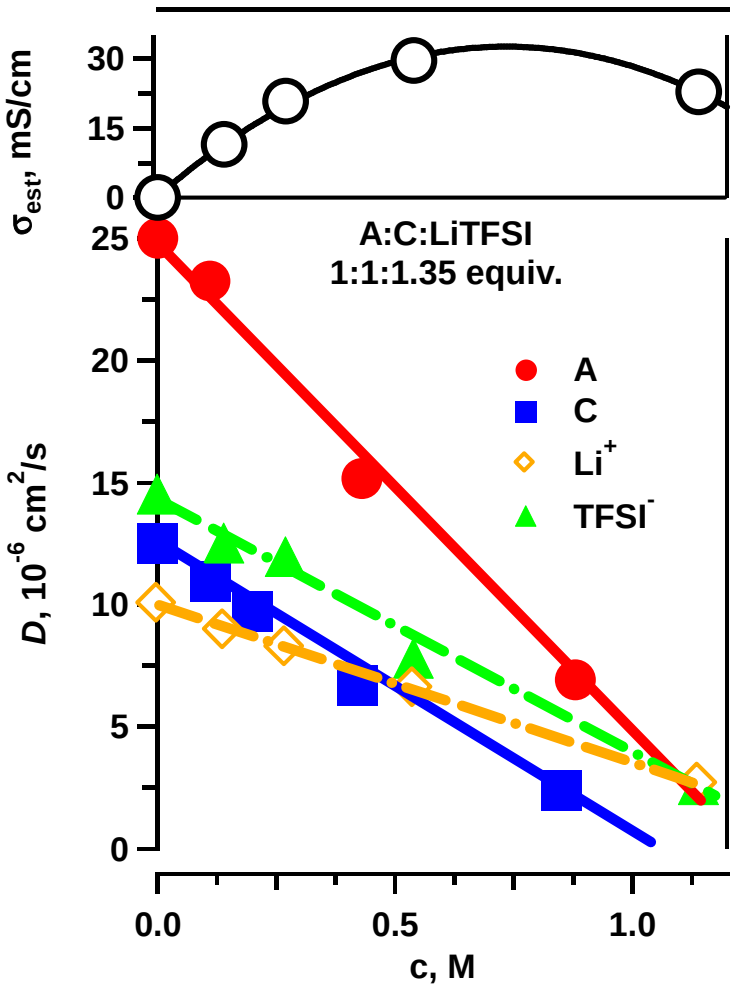

Figure S12. Diffusivity of **A**, **C**, Li^+ and $TFSI^-$ in solutions of 1:1:1.35 equiv. mixture of **A**:**C**:LiTFSI in CD_3CN as a function of [LiTFSI] at 25 °C; proportional dilution (*lower panel*); linear fits. Calculated σ_{est} is shown at the top (*parabolic fit*).

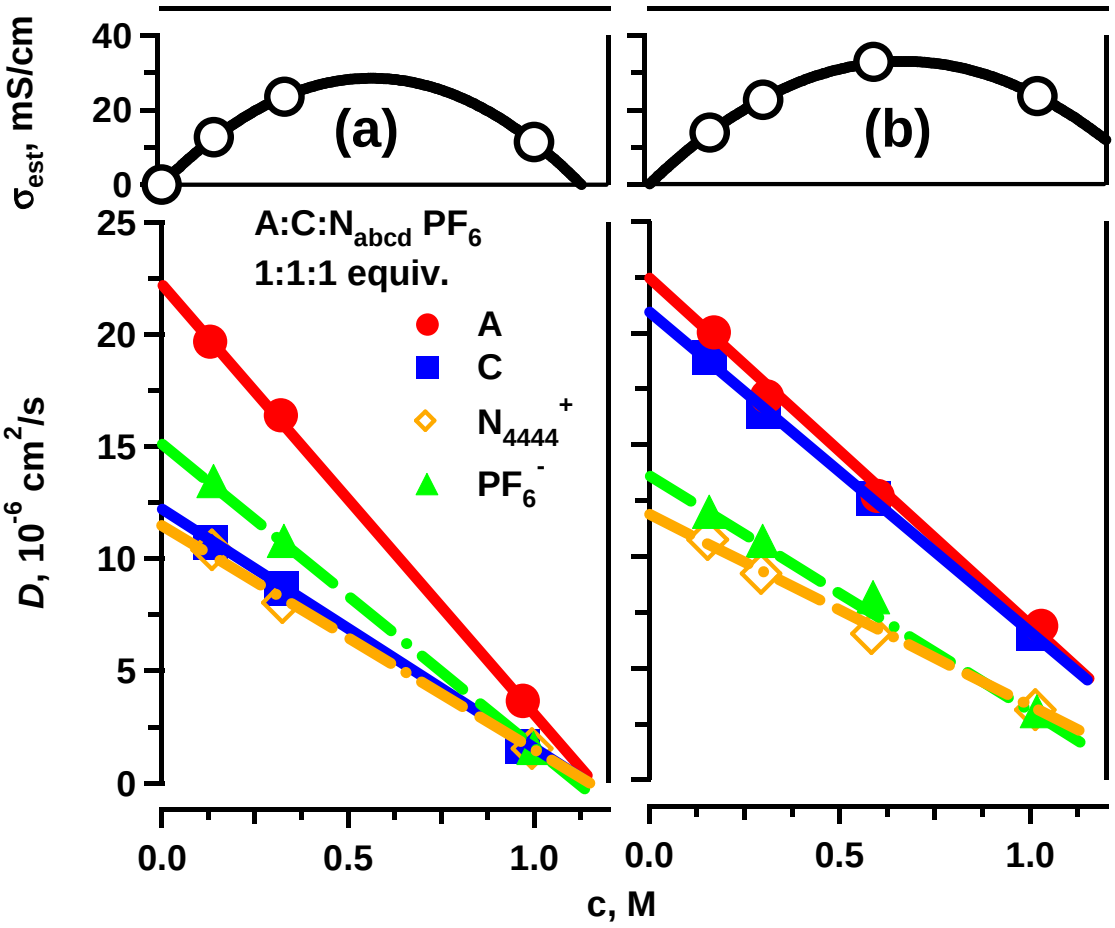

Figure S13. Diffusivity of **A**, **C**, N_{4444}^+ and PF_6^- in solutions of 1:1:1 equiv. mixture of **A**:**C**:N_{4444} PF_6 plotted vs. salt molarity in CD_3CN at 25 °C; proportional dilution (*lower panels*); linear fits. Calculated σ_{est} is shown at the top (*parabolic fits*). In panel b, a small molecule (1,4-dimethoxybenzene) was used as "downsized" a catholyte.

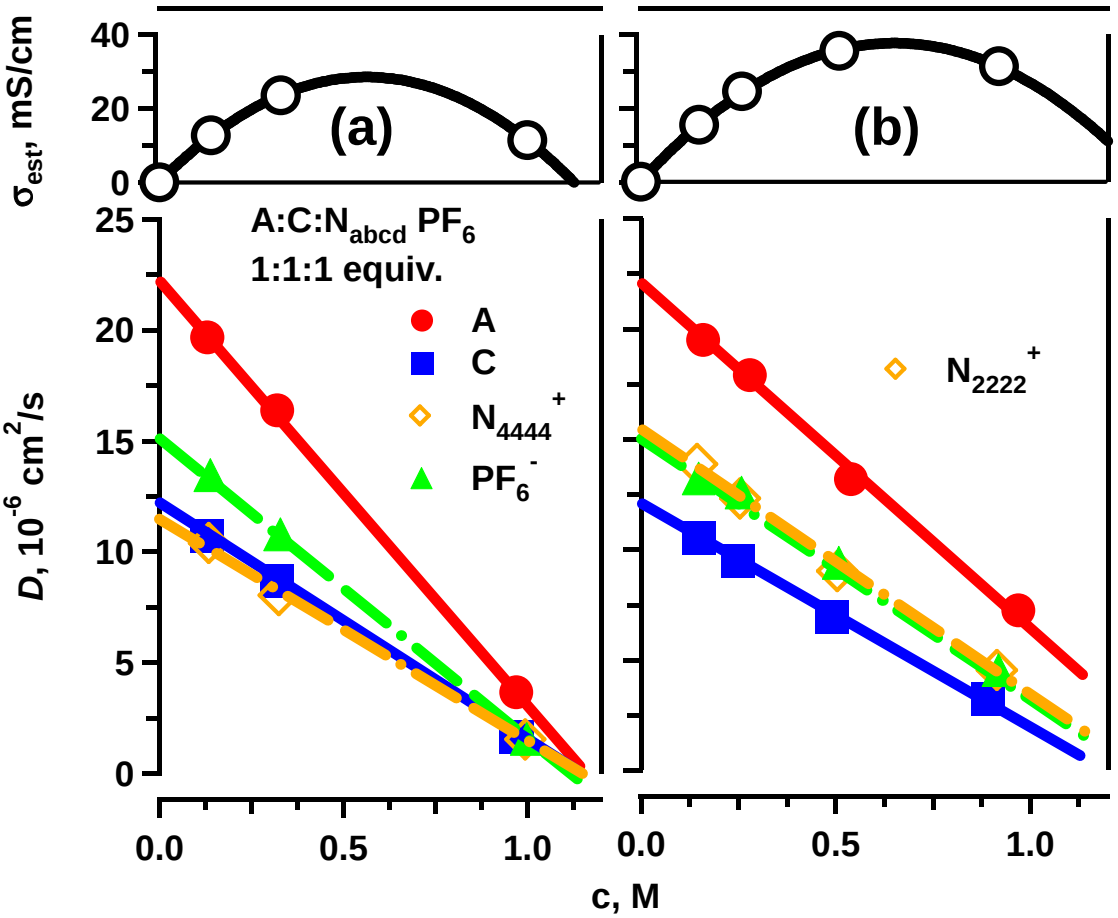

Figure S14. Diffusivities of **A**, **C**, N_{abcd}^+ and PF_6^- in solutions of 1:1:1 equiv. mixtures of (a) **A**:**C**:N_{4444} PF_6 and (b) **A**:**C**:$N_{2222}PF_6$ plotted vs. salt molarity in CD_3CN at 25 °C; proportional dilution (*lower panels*); linear fits. Calculated σ_{est} is shown at the top (*parabolic fits*). Greater diffusivity of the smaller tetralkylammonium cation results in the greater conductivity.

Additional references.

(1) Wu, D.; Chen, A.; Johnson, C. S., Jr. An Improved Diffusion-Ordered Spectroscopy Experiment Incorporating Bipolar-Gradient Pulses. *J. Magn. Res.* **1995,** *115*, 260-264.

(2) Johnson, C. S., Jr. Diffusion Ordered Nuclear Magnetic Resonance Spectroscopy: Principles and Applications. *Prog. Nucl. Magn. Res. Spect.* **1999,** *34*, 203-256.

(3) Landrum, G. RDKit: Open-Source Cheminformatics. http://www.rdkit.org

(4) Moriwaki, H.; Tian, Y.; Kawashita, N.; Takagi, T. Mordred: A Molecular Descriptor Calculator. *J. Cheminform.* **2018,** *10*, 4.

(5) Beckner, W.; Mao, C. M.; Pfaendtner, J. Statistical Models Are Able to Predict Ionic Liquid Viscosity across a Wide Range of Chemical Functionalities and Experimental Conditions. *Mol. Syst. Des. Eng.* **2018,** *3*, 253-263.

(6) Cramer, E. M. Some Symmetric, Invariant Measures of Multivariate Association. *Psychometrica* **1979,** *44*, 43-53.

(7) Tibshirani, R. Regression Shrinkage and Selection via the Lasso. *J. R. Statist. Soc. B* **1996,** *58*, 267-288.

(8) Zou, H.; Hastie, T. Regularization and Variable Selection Via the Elastic Net. *J. R. Statist. Soc. B* **2005,** *67, Part 2*, 301-320.

(9) Broadhurst, D.; Goodacre, R.; Jones, A.; Rowland, J. J.; Kelp, D. B. Genetic Algorithms as a Method for Variable Selection in Multiple Linear Regression and Partial Least Squares Regression, with Applications to Pyrolysis Mass Spectrometry. *Anal. Chim. Acta* **1997,** *348*, 71-86.

(10) Todeschini, R.; Consonni, V., *Handbook of Molecular Descriptors*. Wiley-VCH: New York, 2000.